Ru–Mo/HZSM-5 catalyzed methane aromatization in membrane reactors

F. Larachi [a,c,*], H. Oudghiri-Hassani [b,c], M.C. Iliuta [a,c] B.P.A. Grandjean [a,c], and P.H. McBreen [b,c]

[a] Department of Chemical Engineering, Laval University, Québec, Canada G1K 7P4
[b] Department of Chemistry, Laval University, Québec, Canada G1K 7P4
[c] Research Center for the Properties of Interfaces and Catalysis CERPIC, Laval University, Québec, Canada G1K 7P4

Received 20 June 2002; accepted 28 August 2002

Oxygen-free methane conversion into benzene was carried out in a catalytic membrane reactor over 0.5%Ru–3%Mo/HZSM-5 in the temperature range 873–973 K following three reaction protocols: (i) straight-run catalytic reactor without hydrogen permeation (OFF), (ii) cycled OFF/ON hydrogen permeation sequences, and (iii) cycled OFF/ON hydrogen permeation sequences intertwined with CH_4/H_2 regenerative steps. X-ray photoelectron spectroscopy analysis of fresh and spent catalysts identified, in all cases, three types of carbon species that formed during aromatization, including carbide formation. The presence of a permeating membrane did not give rise to different chemical states of carbon and molybdenum on the catalyst from those known to form in straight runs under no hydrogen permeation. The ON mode, *i.e.*, during permeation, led to the accumulation of graphite-like and aromatic-aliphatic (coke) species on the catalyst. However, both types of carbon were reduced during the OFF step either by autogenous hydrogen or *via* an external source of hydrogen under CH_4/H_2 regenerative steps.

KEY WORDS: molybdenum carbide; methane nonoxidative aromatization; catalytic membrane; surface analysis; zeolite catalysis.

1. Introduction

The application of membrane reactors for methane dehydrocyclization (or aromatization) has been receiving greater attention in the past few years, particularly over Ru-doped molybdenum-containing HZSM-5 catalysts [1–3]. Membrane reactors are devices that exploit the perm-selective separation function of a membrane to imbalance favorably the species concentration distribution within equilibrium-controlled *reaction* media. The advantage behind their use in aromatization is double since they provide high-purity hydrogen as a valuable byproduct and effect the conversions into aromatics, of cheap and abundant methane, that surpass the *equilibrium* conversion bottleneck [4–6].

Due to endothermic and equilibrium-controlled factors, methane conversion into aromatics is severely limited at low temperatures. Therefore, temperatures in excess of 973 K are required to boost it to meaningful levels within conventional fixed-bed catalytic reactors. Most of the experimental studies reported in the literature were performed at 973 K or above. Nonetheless, high-temperature operation is known to lead to serious deactivation of Mo-based catalysts by coke deposition and/or by Mo loss through volatilization [7]. Coke deposition is one important drawback to methane aromatization that is responsible for the decrease in conversion into useful products. Therefore, much of the current work has been targeted at improving conversion into aromatics and reducing coke formation [7–16].

A tremendous amount of characterization work has been reported on both molybdenum and carbon in the zeolite-supported catalyst as well as on the modes of methane activation in conventional catalytic reactor operation [8,9,17–22]. There is evidence that Mo^{6+} available in the zeolite channels, likely as MoO_3 [21–23], are reduced during an induction period by CH_4 into active Mo_2C species [18]. These in turn are considered to be the initiating sites for the formation of ethylene and other primary products which further convert into aromatics on the zeolite acidic sites. There is some speculation that carbene intermediates are involved in the aromatization process [24,25]. Recent work by Zahidi *et al.* [26] shows that carbene species are in fact stable on Mo_2C to the very high temperatures required for the reaction.

Methane aromatization over 0.5%Ru–3%Mo/HZSM-5 was implemented in a membrane catalytic reactor to evaluate whether or not both conversion into aromatics and reduction of coke could be ameliorated with respect to the conventional route in fixed-bed catalytic reactors. Besides Mo, Ru was co-impregnated onto Mo/HZSM-5 to promote both conversion into benzene and catalyst stability [13]. The possible functions ascribed to ruthenium, and that have indeed been speculated to affect methane aromatization, are reflected in the modulation of the population of

* To whom correspondence should be addressed.
E-mail: flarachi@gch.ulaval.ca

1011-372X/02/1200-0183/0

strong acid sites, in the promotional effect on the reduction of molybdenum species and in the enhancement of the catalyst capacity to cleave C–H bonds in CH_4, to name just a few functions [13]. By continuously removing co-produced hydrogen, the equilibrium-limited reaction is expected to shift towards the formation of aromatics. However, removal of hydrogen might also be expected to favor coke deposition. The present study will attempt therefore to address the following two issues:

- Does the presence of a permeating membrane give rise to chemical states of carbon and molybdenum different from those already known to form in straight runs under no H_2 permeation?
- Can the deposited carbon be reduced by hydrogen when permeation is interrupted either by using an autogenous or an external H_2 source such as under CH_4/H_2 regenerative steps?

2. Experimental

2.1. Preparation and pretreatment of Ru–Mo/HZSM-5

A 0.5%Ru–3%Mo/HZSM-5 catalyst was prepared by incipient wetness co-impregnation of the ammonium form of the zeolite [NH_4ZSM-5] (Si/Al = 15) using the required amount of aqueous ammonium heptamolybdate [$(NH_4)_6Mo_7O_{24}{\cdot}4H_2O$] and ruthenium chloride [1]. The catalyst was air-dried for 12 h at ambient temperature, then for 2 h at 393 K and was finally air-calcined for 4 h at 873 K. The solid samples were pressed, crushed, and sieved to isolate catalyst granules in the size range 20–35 mesh for subsequent use in the methane aromatization reactions. Before exposure to methane, the catalyst underwent pretreatment consisting of gradual heating under argon in temperature-ramped mode up to 873 K and maintained at this temperature for 4 h. Then, the catalyst was treated in flowing air for 30 min at 973 K and in pure hydrogen at 573 K.

2.2. Preparation of β-Mo_2C

Molybdenum carbide polycrystalline β-Mo_2C samples were prepared by Oyama [27] by carburizing pure Mo metal foils in a temperature-program-controlled quartz reactor fed at a volumetric flow rate of 300 ml/min with a 20:80 v/v% CH_4:H_2 mixture. The samples were exposed to flowing gas while starting a linear temperature program at a heating rate of 8 K/min up to 1373 K, where they were kept for 3 h to complete the reaction. The X-ray diffractograms of carburized foils confirmed that the samples were essentially pure bulk β-Mo_2C [28]. The foil was then mounted on a tantalum plate for resistive heating under ultra-high vacuum (UHV) conditions [29]. Sulfur contamination from the Mo_2C surface was removed by repeated cycles of argon sputtering at 500 K and annealing to 1300 K. Residual oxygen was removed by depositing carbon on the surface *via* the decomposition of ethylene or propylene at 500–600 K and heating to 1300 K. The XPS analysis of the carbide freshly introduced in the UHV revealed an intense C 1s peak at 284.5 eV and a shoulder at 283 eV. Simple heating to 1300 K removes the peak at 284.5 eV, leaving only the carbidic carbon C 1s signal. Furthermore, heating to 1300 K removes most of the O 1s signal, leaving a weak peak at 530.0 eV.

2.3. Catalytic testing and product analysis

Figure 1 is a sketch of the catalytic membrane reactor and its ancillary accessories. It consists of a 17 mm i.d. tube reactor hosting a 70 mm long and 9.5 mm o.d. Pd/Ag homemade tubular membrane prepared by electroless plating on the outer shell of a *porous* stainless steel

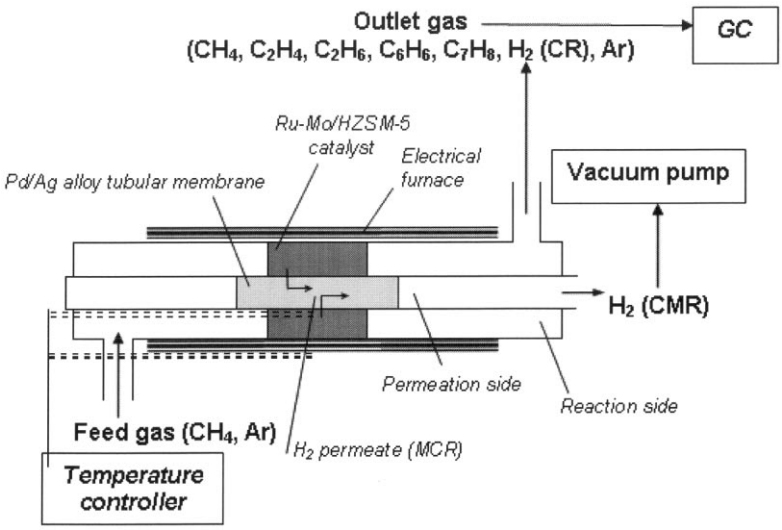

Figure 1. Experimental setup.

tube [2]. The reactor was loosely packed with 3 g of 0.5%Ru–3%Mo/HZSM-5 catalyst and connected to a gas-feeding unit and analytical equipment. The reaction temperature, kept at 873, 923, and 973 K, was controlled by means of a sheathed thermocouple immersed in the 35-mm-high catalyst layer. After catalyst pretreatment, a 90:10 v/v% methane:Ar mixture was fed to the reactor at a mass-flow controlled rate of 270 ml (STP) h^{-1} g^{-1} methane hourly space velocity. All methane aromatization tests were run at atmospheric pressure.

A vacuum pump connected to the permeation zone maintained *ca.* 0.2 kPa pressure to provide sufficient driving force for evacuating, out of the reaction zone, H_2 produced from the aromatization.

The reaction gas products were analyzed by means of a Perkin–Elmer gas chromatograph equipped with a flame ionization detector connected to a GS–Q capillary megabore column (30 m long and 530 μm i.d.), and with a thermal conductivity detector connected to a Carboxen 1010 capillary column (30 m long and 530 μm i.d.). The following gas products were analyzed in the reactor exit stream: benzene, toluene, ethylene, and ethane. Benzene was the major hydrocarbon product, whereas naphthalene was detected in trace amounts mainly during membrane operation. Though the catalyst deactivation by coke deposits was noticeable, the amount of deposited carbon was found to be marginal with respect to that contributing to the gas products. Typically, after *ca.* 4000 min on-stream of reaction, whether permeation was ON or OFF, the increase in catalyst weight represented less than 0.1% of the carbon contained in the total amount of methane used at 873 K and only about 0.2% at 973 K. Methane conversion was thus calculated based on the carbon content of benzene, toluene, ethylene, and ethane. As benzene was the most dominant gas-product species, methane conversion was simply equated with benzene formation.

2.4. Catalyst characterization

X-ray photoelectron spectra (XPS) for the fresh and spent 0.5%Ru–3%Mo/HZSM-5 catalyst samples were acquired at room temperature using a Vacuum Generators Scientific ESCALAB Mark II system and non-monochromatized Mg K_α ($h\nu = 1253.6$ eV) and Al K_α ($h\nu = 1486.6$ eV) X-ray radiation. The latter source was used to avoid the partial interference between the C 1s region excited by the Mg K_β and the Mo 3d region. The source, operated at 50 W, probed an 800-μm diameter spot on the powdered samples. The photoelectron kinetic energies were measured using a hemispherical electrostatic analyzer working in the constant pass energy mode. The background pressure in the analyzing chamber was kept below 7.5×10^{-8} torr. Survey scans (0–1150 eV) and high-resolution Mo 3d, C 1s and O 1s spectra were acquired at a pass energy of 20 and 15 eV, respectively. Correction for charging effects was effected by referencing all binding energies with respect to the Si 2p core level spectrum in SiO_2 (BE $\approx$ 103.4 eV). For all acquired spectra, the uncertainty in peak position was estimated to be $\pm$0.2 eV. Typically up to 1000 scans for Mo 3d, 100 for C 1s, and 10 for O 1s were acquired to achieve acceptable signal-to-noise levels.

XPS measurements of the reference β-Mo_2C samples were performed in a different UHV chamber where the background pressure was below 2×10^{-10} torr. The Mo 3d and C 1s core-level spectra were referenced with respect to the Fermi level for the β-Mo_2C samples and acquired at a pass energy of 15 eV for Mo 3d and 10 eV for C 1s.

The analysis of the measured Mo 3d, C 1s, and O 1s high-resolution spectral envelopes was performed by curve-fitting synthetic peak components using the XPSPEAK41 and Origin 6.0 Peak Fitting software. The raw experimental data were used with no preliminary smoothing. Gaussian–Lorentzian product functions were used to approximate the line shapes of the fitting components. Shirley (Ru–3Mo/HZSM-5) or cubic-spline (β-Mo_2C) background subtraction procedures were used. Quantification of the Mo and C atomic percentages was obtained from integration of the Mo 3d and C 1s core-level spectra with the appropriate corrections for photo-ionization cross-sections.

3. Results and discussion

The aromatization reaction was run following three modes. In *catalytic reactor* (CR) mode (OFF mode), the vacuum pump was off and hydrogen was not allowed to permeate across the membrane while methane was undergoing conversion in the catalyst bed. In *catalytic membrane reactor* (CMR) mode (ON mode), hydrogen was allowed to bleed through the membrane, thus shifting the equilibrium-controlled methane aromatization reaction towards benzene formation. Finally a CR(H_2) regenerative mode was used in which the catalyst bed was reactivated by exposure, for a brief period of time, to a CH_4/H_2 mixture. This allowed restoration of the coke-deactivated sites [19] that had been poisoned in earlier CMR modes of the catalyst bed.

3.1. Catalytic reaction results

The catalytic tests were conducted according to three protocols: straight-run CR, cycled CR/CMR, and cycled CR/CMR/CR(H_2).

Consistent with previous observations [1,17–19], CH_4 conversion over Mo-containing HZSM-5 catalysts in an oxygen-free environment is characterized by an induction period prior to the formation of benzene, toluene, and naphthalene. The induction period corresponds to the reduction by CH_4 of Mo(VI) in the zeolite to active Mo carbides [18,19]. Figure 2(a) shows that in the

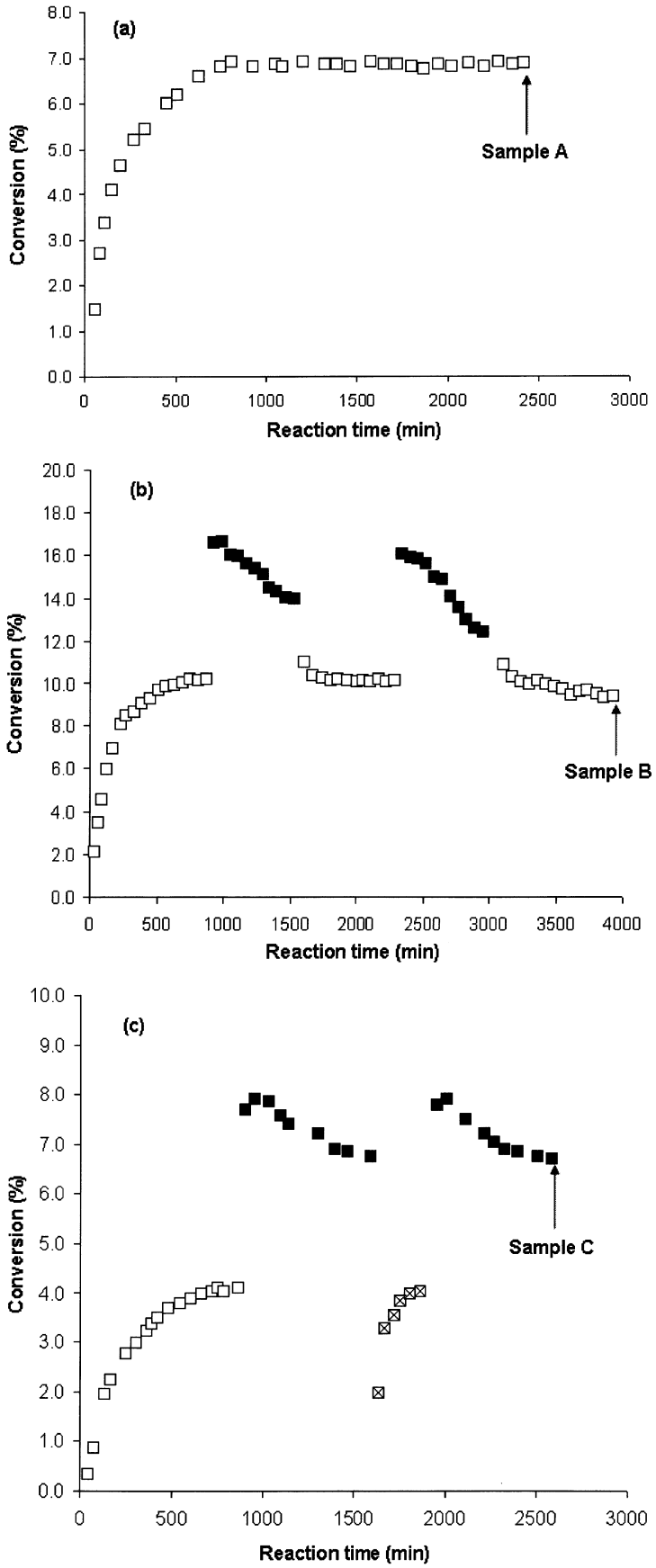

Figure 2. Methane conversion over 0.5%Ru–3%Mo/HZSM-5 catalyst at 270 ml (STP) h^{-1} g^{-1} (a) without hydrogen permeation (CR mode) at 923 K, (b) cycled CR/CMR mode at 973 K, (c) cycled CR/CMR/CR(H_2) mode at 873 K.

absence of H_2 permeation (CR mode), once the induction period is over, the Ru–Mo/HZSM-5 catalyst activity levels off at about 7% CH_4 conversion at 923 K and 270 ml (STP) h^{-1} g^{-1} methane hourly space velocity. This methane conversion amounts to 86% of the thermodynamic equilibrium conversion at the same temperature.

In accordance with our previous work [1,3], lower methane space velocities induced longer induction periods but higher ultimate (or plateau) methane conversions. The effect of hydrogen permeation on methane conversion was found to be quite modest at methane space velocities above *ca.* 600 ml (STP) h^{-1} g^{-1} [1] for which both CR and CMR modes yielded almost identical conversions. The CMR mode became more advantageous for methane space velocities below 400 ml (STP) h^{-1} g^{-1}. Therefore, the reaction tests reported here were carried out at a methane space velocity of 270 ml (STP) h^{-1} g^{-1}.

Figure 2(b) shows the time evolution of CH_4 conversion during cycled CR/CMR at 973 K. In switching from CR to CMR by establishing hydrogen permeation, methane conversion exhibited a sharp overshoot and attained about 17%. This peak in conversion represented 150% of the thermodynamic conversion at 973 K. This phenomenon is easily explained by the equilibrium shift toward products triggered by hydrogen starvation in the reaction zone. The conversion peak was rapidly supplanted by a steady decrease ascribed to the build-up of coke deposits (CMR coke) that impeded access to the active sites. When switching from CMR back to CR, a very sharp fall-off in conversion took place. However, the conversion quickly stabilized to its CR plateau conversion value. This suggests that the CMR coke did not alter permanently the active sites so that the build-up of *autogenous* hydrogen in CR mode could remove an important proportion of it. The kinetics of replenishment of the active sites through re-hydrogenation of carbonaceous species depends on the amount of hydrogen becoming available with the progress of methane conversion, and consequently on the time span allowed for CR mode operation before CMR is resumed afresh. Hence, due to incomplete re-hydrogenation, accumulation of persistent residual CMR coke yields progressively lower peak conversions (figure 2(b)).

Compressing the CR time span during which replenishment of active sites takes place is desirable for productivity reasons. This task can be accomplished, without sacrificing high conversion, through addition of hydrogen to the feed stream for a brief time period as shown in figure 2(c). Hence if hydrogen coming from an external source yields qualitatively the same effect as the *in situ* produced hydrogen (figures 2(a), (b)), quantitatively the peak conversions can be restored at the same levels over regenerative CR(H_2) spans much shorter than normal CR spans. Ample evidence of the beneficial action of exogenous hydrogen to quickly restore activity is discussed at length in our previous paper [1].

3.2. XPS analysis

XPS analysis was performed on spent catalyst samples at the end of the experiments. Sample A was withdrawn after 2500 min on-stream in a straight-run CR at 923 K (figure 2(a)). Spent catalyst sample B was for the methane aromatization reaction in cycled CR/CMR mode at 973 K after 4000 min (figure 2(b)), and sample C corresponded to cycled CR/CMR/CR(H_2) reaction at 873 K after 2700 min (figure 2(c)). The calcined non-reduced catalyst before reaction and the β-Mo_2C sample are referred to as samples O and β, respectively. The latter sample was used as a reference to assign the binding energies corresponding to carbidic molybdenum and carbidic carbon.

The XP core-level spectra of Mo 3d, O 1s, and C 1s in samples β, O, and A–C are shown as a matrix-plot in figure 3. From the analysis of the near-surface atom compositions it was observed that the reaction temperature and the amount of molybdenum detected in the catalyst outermost layers were negatively cross-correlated. Conversely, temperature and carbon intensity were positively cross-correlated. Table 1 provides a compilation of the energy assignments of the spectral components in all analyzed high-resolution XPS data. Table 2 contains data on the *post facto* verification of the consistency of the XPS curve fitting and deconvolution. Finally, table 3 provides the relative intensities of the carbidic Mo with respect to total Mo, and of the different carbon constituents in the C 1s spectral envelopes. It is worth noting that the relative amount of carbidic molybdenum with respect to total Mo is an increasing function of temperature.

The XPS data for β-Mo_2C indicate the presence of Mo $3d_{5/2}$ and Mo $3d_{3/2}$ spin–orbit doublets characteristic of carbidic molybdenum with BEs equal to 227.9 and 231.1 eV, fwhm = 1.2 eV (table 1) [28]. Cleaning the molybdenum carbide foil by repeated annealing under UHV conditions at 1300 K was efficient to remove parasitic carbon contributions that might interfere with the C 1s carbidic signature. Hence, as shown in figure 3, only the C 1s peak characteristic of carbidic carbon (BE = 283.0 eV, fwhm = 1.0 eV) remained after several annealing cycles. The residual oxygen content of sample β was very marginal inducing no *oxidic* shift in the Mo 3d peak. The Mo/C stoichiometric ratio calculated from the measured Mo $3d_{5/2}$ and Mo $3d_{3/2}$ intensities with respect to the C 1s intensity was equal to two, which is the expected value for pure Mo_2C species (table 2). In what follows, these binding energies for Mo 3d and C 1s are taken as the fingerprints for the carbidic species that might form in the aromatization of methane over 0.5%Ru–3%Mo/HZSM-5 following the above three reaction policies.

The Mo 3d XP spectrum of the 0.5%Ru–3%Mo/HZSM-5 non-prereduced catalyst, *i.e.*, the calcined precursor (sample O, figure 3), exhibited a double-peaked

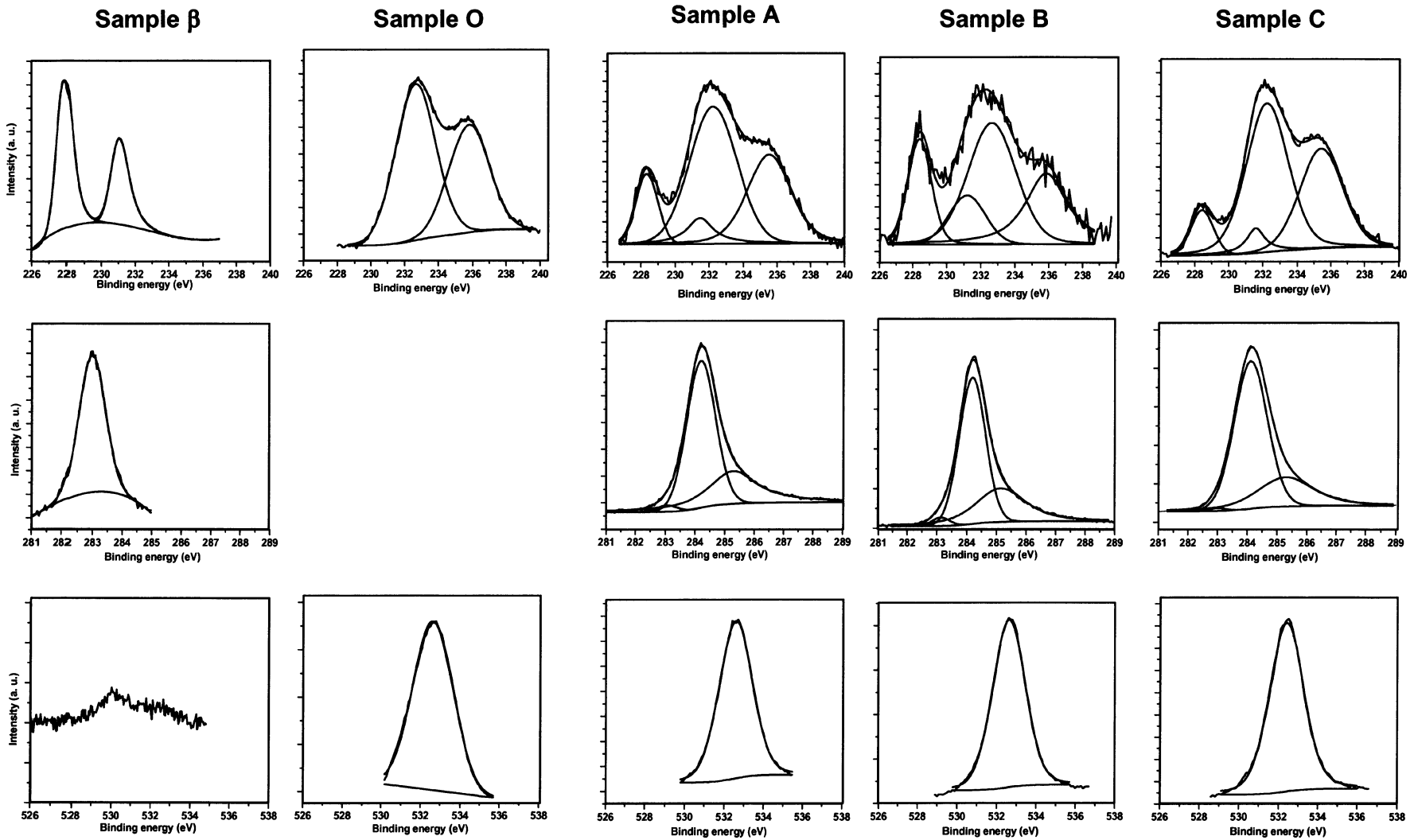

Figure 3. Row-wise Mo 3d, C 1s, and O 1s X-ray photoemission spectra, and column-wise respectively for samples β, O, A, B, and C. Plotted on the figures are the measured spectrum, the smooth simulated individual peak contributions and the sum of all contributions.

Table 1
Energy assignments of the spectral components in Mo $3d_{5/2}$ and Mo $3d_{3/2}$ and C 1s and O 1s observed in β-Mo_2C and Ru–Mo/HZSM-5: fresh (sample O), CR mode (sample A), cycled CR/CMR modes (sample B) and CR/CMR/CR(H_2) mode (sample C).

Sample	Carbidic Mo		Oxidic Mo		C 1s			O 1s
	Mo $3d_{5/2}$	Mo $3d_{3/2}$	Mo $3d_{5/2}$	Mo $3d_{3/2}$	Carbide $\mathbf{C}_1$	Graphite $\mathbf{C}_2$	Aromatic $\mathbf{C}_3$	
β-Mo_2C	227.9	231.1	–	–	283.0	–	–	–
O	–	–	232.6	235.8	–	–	–	532.6
A	228.3	231.4	232.2	235.5	283.0	284.2	285.3	532.6
B	228.4	231.2	232.6	235.8	283.1	284.2	285.1	532.6
C	228.4	231.6	232.3	235.4	283.0	284.1	285.3	532.4

BE shift in eV.

Table 2
Post facto verification of XPS fit consistency.

Sample	Carbidic Mo	Oxidic Mo	Carbidic Mo/$\mathbf{C}_1$	
	Area ratio $3d_{5/2}:3d_{3/2}$	Area ratio $3d_{5/2}:3d_{3/2}$	Area ratio Mo $3d_{5/2}$: C 1s	Area ratio Mo $3d_{3/2}$: C 1s
β-Mo_2C	1.4	–	2.0	2.1
O	1.4	–	–	–
A	1.5	1.5	2.0	2.0
B	1.5	1.5	2.0	2.0
C	1.5	1.5	2.0	2.0

envelope and BEs characteristic of Mo(VI), table 1. The observed binding energies closely matched those reported by Solymosi *et al*. [20] for MoO_3 deposited on HZSM-5. The dominance of valence +6 Mo is also in agreement with that observed by Lunsford and coworkers for freshly calcined 2%Mo/HZSM-5 catalysts [18,19] and by Wong *et al*. [30] for 3%Mo/HZSM-5. In our case, it is likely that Mo(VI) exists as MoO_3 inside the zeolite [18,21,22,30]. The O 1s XP spectrum was fitted with a single peak at 532.8 eV (table 1) due to silicon oxide [31], *i.e*., the most abundant oxide.

After the pretreatment in argon, air and then H_2, the catalyst was exposed to methane at 923 K for 2500 min in CR mode, and sample A was taken in steady-state operation and transferred in air to the XPS vacuum chamber. The inception of a new doublet characteristic of the carbide indicates the partial reduction of the original Mo(VI) species. Such incomplete carburization of Mo under a CH_4 stream was also reported by Lunsford and coworkers [19], although it was reported by them that hexavalent Mo reduced almost completely into carbidic Mo and oxidic Mo(IV) and Mo(V) within 2 h at 973 K for the 2%Mo/HZSM-5 catalyst. Reduction of 2%Mo/HZSM-5 with CO at 973 K was also observed to lead to multiple bands characteristic of a mixture of Mo(VI) and carbidic Mo [8]. XRD characterization of H_2/n-C_4 *in situ* activated MoO_3/HZSM-5 showed the formation of molybdenum oxycarbide species exhibiting $MoO_{2.42}C_{0.23}H_{0.78}$ *bulk* stoichiometry [22]. The C 1s spectrum of sample A was fitted to three peaks for carbons of a carbidic type ($\mathbf{C}_1$, BE = 283.0 eV, fwhm = 1.0 eV), graphite-like carbon ($\mathbf{C}_2$, BE = 284.2 eV, fwhm = 1.1 eV) and carbon of an aromatic–aliphatic type in small compounds ($\mathbf{C}_3$, BE = 285.3 eV, fwhm = 2.0 eV) [31,32] (see figure 3). Assignment of the latter species was motivated by the detection of naphthalene as one of the gas products, knowing that the formation of condensed aromatics is one of the routes to coke formation. Based on the overall appearance and contributions to the fitted spectra of figure 3, it is also equally statistically likely to obtain an acceptable fit using only the two dominant $\mathbf{C}_2$ and $\mathbf{C}_3$ features. However, this combination is to be ruled out because of evidence of the existence of a carbidic contribution stemming from the XP spectrum of the Mo 3d region as confirmed by the *post facto* statistics of table 2. Moreover, oxygen-bearing carbon was not observed. Therefore, a three-carbon peak reconstruction as in figure 3 is judged to be a physically sound choice. The peak for graphitic carbon was the most intense; it was accompanied by a weaker aromatic–aliphatic peak and then by a barely visible carbidic peak, which is

Table 3
Relative intensities (%) of Mo 3d and C 1s species.

Sample	Carbidic Mo	$\mathbf{C}_1$	$\mathbf{C}_2$	$\mathbf{C}_3$
β-Mo_2C	100.0	100.0	–	–
O	0.0	0.0	–	–
A	18.8	1.8	63.6	34.5
B	29.8	2.3	62.8	34.9
C	13.0	0.7	70.3	29.0

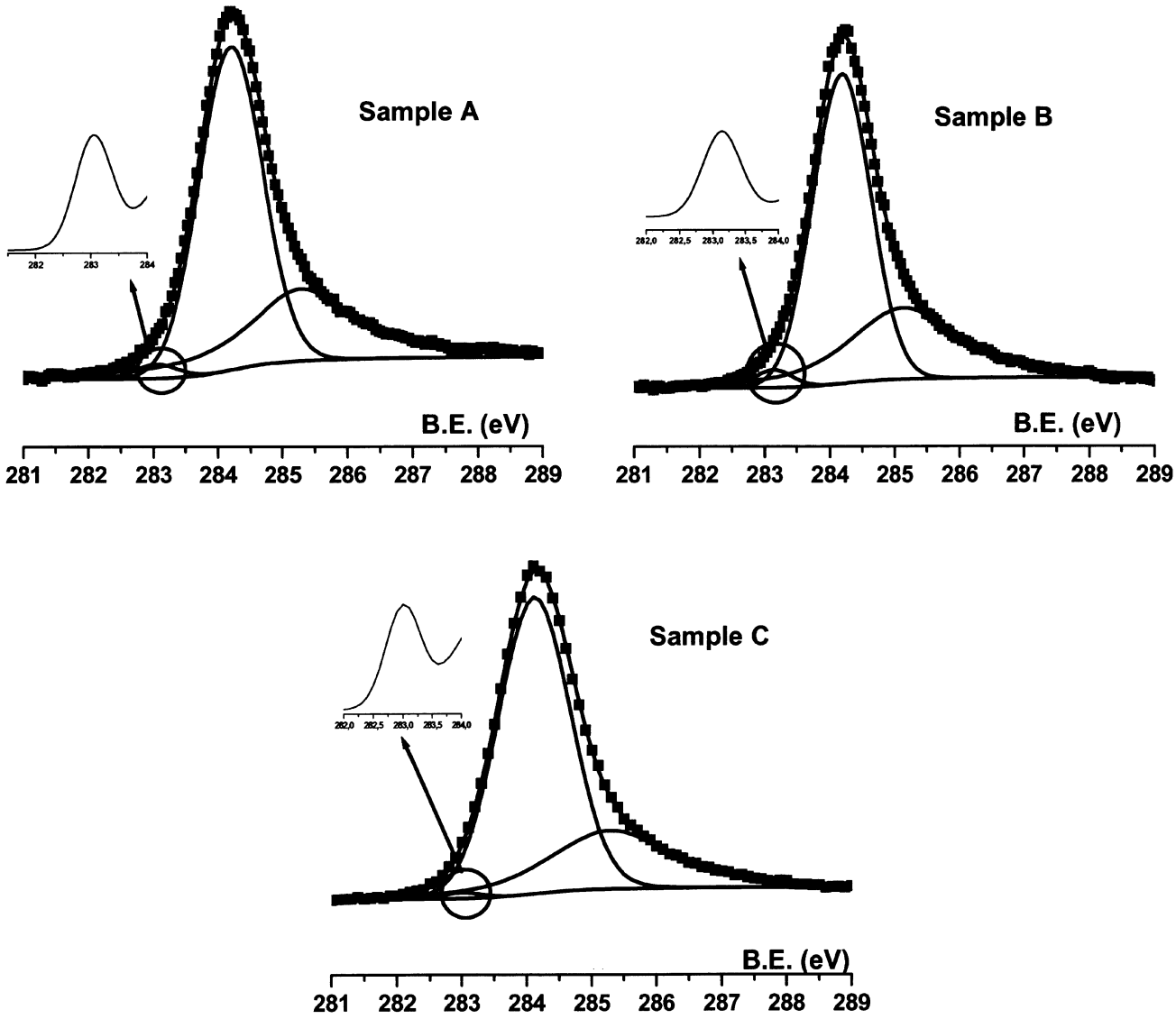

Figure 4. XP C 1s spectra zoomed out for showing the details of the carbidic contributions for samples A, B, and C.

zoomed out for detail in figure 4. Though *ca.* 80% of the Mo XPS signal is for MoO_3, after 2500 min on-stream, the stoichiometric ratio of carbidic Mo to $\mathbf{C}_1$, as illustrated in table 2, is consistent with Mo_2C. Mo^0 cannot be distinguished from Mo_2C on the basis of Mo 3d binding energy measurements alone, but the presence of Mo^0 is ruled out on the basis of the observed Mo_2C stoichiometric ratio [19]. This conclusion is roughly consistent with X-ray absorption spectroscopy (XAS) data by Ding *et al.* [24] showing the formation of 0.6–1.0 nm MoC_x clusters in active Mo/H-ZSM5 methane aromatization catalysts. The area under the deconvoluted spectrum representing carbidic Mo in sample A (figure 3) was 18.8% (table 3) of the total Mo 3d signal. The mixture of carbide and oxide signals results in part from the fact that the sample is exposed to air prior to XPS analysis, given that XPS is a surface-sensitive technique. Hence, we simply point out that the effective or averaged stoichiometry, as detected by XPS measurements, is $MoO_{2.42}C_{0.38}$.

The binding energies corresponding to carbidic Mo $3d_{5/2}$ and Mo $3d_{3/2}$ were registered respectively at 228.3 and 231.4 eV (table 1). These BEs exhibited a slight shift to higher binding energies compared to those in sample β, which is possibly ascribed to differences between the powder-supported molybdenum carbide and the unsupported β-Mo_2C foils. However, the binding energies for carbidic Mo in sample A were found to agree well with literature data on the treatment of MoO_3/HZSM-5 with methane at 973 K for 2 h [19,20]. They were also found to be consistent with those for pure powdered unsupported Mo_2C [19].

Exposure of 0.5%Ru–3%Mo/HZSM-5 to cycled CR/CMR sequences at 973 K for 4000 min on-stream results in the accumulation of a significant amount of coke, especially in the CMR mode, due to methane conversion

intensification. The coke deposits on the catalyst decreased the near-surface Mo concentration by a factor of six with respect to the original non-prereduced catalyst, thereby accounting for the very weak Mo 3d signal (sample B, figure 3). In comparison to straight-run CR sample A, the higher temperature in this case yielded a greater relative proportion of carbidic molybdenum with respect to total XPS-probed Mo (table 3). This corresponded to an effective or averaged near-surface stoichiometry of $MoO_{2.1}C_{0.60}$. Interestingly, the percentage of $\mathbf{C}_2$ and $\mathbf{C}_3$ contributions in C 1s barely varied between the two experiments, *i.e.*, $\mathbf{C}_2 + \mathbf{C}_3 \approx 98\%$. It is hence likely that in CR mode the shadowing effect of coke on the carbidic sites would be less dramatic than in the case of CMR mode because autogenous H_2 contributes to hydrogenate, and thus to partially remove, the incipient coke.

Deconvolution of the C 1s core-level spectrum for sample C taken in CMR operation showed that when hydrogen permeates through the membrane, 99.3% of the carbon is non-carbidic, confirming the tendency of the catalyst to rapidly deactivate in H_2-starved conditions. The lower reaction temperature, 873 K, resulted in the reduction of only 13% of the molybdenum species into Mo_2C (table 3). The remaining molybdenum was occurring in the +6 state (figure 3) yielding an effective or averaged surface stoichiometry of $MoO_{2.6}C_{0.26}$.

4. Conclusions

The catalyst, subjected to aromatization up to 70 h of continuous operation, exhibited high conversion overshoots in CMR steps and excellent stability in CR steps where native hydrogen was believed to reactivate the catalyst through removal of coke-type carbon. Addition of hydrogen in the feed stream was observed to reduce the span of CR steps by quickly reactivating the catalyst. The XPS study of fresh and spent catalysts showed that three different kinds of carbon species were formed during aromatization: carbidic carbon at 283.0 eV, graphite-like carbon at 284.2 eV (the most prominent carbon species), and aromatic–aliphatic species at 285.3 eV. The molybdenum evolved from the +6 state in the oxide toward the carbidic state in Mo_2C, but no more than 30% Mo(VI) were converted into carbidic Mo, suggesting that non-stoichiometric oxycarbides form at least in the near-surface region, during the catalytic reaction. The binding energies of carbidic carbon and molybdenum were referenced using the XPS features in β-Mo_2C obtained by carburizing pure metallic molybdenum foils in CH_4/H_2. The presence of a permeating membrane did not modify the chemical states of carbon and molybdenum on the catalyst surface which shared the same features as in the conventional CR mode. However, it was observed that permeation favored the accumulation of graphite-like and aromatic–aliphatic (coke) species that are responsible for the loss in catalyst activity. Nonetheless, both carbon types were reduced during CR steps owing either to the build-up of autogenous hydrogen or to an external source of hydrogen.

In summary, the following conclusions can be drawn:

1. The conversion of methane, mainly into benzene, over supported Ru–Mo/HZSM-5 catalyst was observed to take place at meaningful levels at temperatures as low as 873 K in the presence of a permselective membrane allowing evacuation of hydrogen from the reaction zone. The equilibrium-controlled reaction was shifted toward the products attaining peak conversions up to twice the theoretical equilibrium conversion at 270 ml (STP) h^{-1} g^{-1} methane hourly space velocity.
2. The formation of hydrocarbons, and particularly benzene, was accompanied by the reduction of the oxidic hexavalent molybdenum into carbidic molybdenum regardless of whether or not the membrane permeation was ON or OFF.
3. In ON membrane operation the boost in conversion was offset by an immediate drop-off ascribed to an accelerated build-up of non-carbidic carbon on top of the methane-activating Mo_2C sites.
4. The previous non-carbidic coke was reversible and in OFF membrane operation or during the CH_4/H_2 regenerative step, the availability of H_2 helped its re-hydrogenation and restoration of the active sites.

Acknowledgment

The authors would like to thank Dr. A. Adnot for his assistance in the XPS study.

References

[1] M.C. Iliuta, F. Larachi, B.P.A. Grandjean, I. Iliuta and A. Sayari, Ind. Eng. Chem. Res. 41 (2002) 2371.
[2] M.C. Iliuta, B.P.A. Grandjean and F. Larachi, Ind. Eng. Chem. Res., submitted June 2002.
[3] O. Rival, B.P.A. Grandjean, C. Guy, A. Sayari and F. Larachi, Ind. Eng. Chem. Res. 40 (2001) 2212.
[4] N. Jemaa, B.P.A Grandjean and S. Kaliaguine, Can. J. Chem. Eng. 73 (1995) 405.
[5] A. Li, W. Liang and R. Hughes, J. Membr. Sci. 49 (1998) 259.
[6] V. Höllein, M. Thornton, P. Quicker and R. Dittmeyer, Catal. Today 33 (2001) 33.
[7] J.L. Zeng, Z.T. Xiong, H.B. Zhang, G.D. Lin and K.R. Tsai, Catal. Lett. 53 (1998) 119.
[8] B.M. Weckhuysen, M.P. Rosynek and J.H. Lunsford, Catal. Lett. 52 (1998) 31.
[9] Y. Xu and L. Lin, Appl. Catalysis A: General 188 (1999) 53.
[10] L. Chen, L. Lin, Z. Xu, T. Zhang and X. Li, Catal. Lett. 39 (1996) 169.
[11] L. Wang, Y. Xu, S.T. Wong, W. Cui and X. Guo, Appl. Catal. A: General 152 (1997) 173.
[12] S. Liu, Q. Dong, R. Ohnishi and M. Ichikawa, Chem. Commun. 1997, 1455.
[13] Y. Shu, Y. Xu, S.T. Wong, L. Wang and X. Guo, J. Catal. 170 (1997) 11.

[14] H. Jiang, L. Wang, W. Cui and Y. Xu, Catal. Lett. 57 (1999) 95.
[15] S. Liu, Q. Dong, R. Ohnishi and M. Ichikawa, Chem. Commun. 1998, 1217.
[16] P. Tan, Z. Xu, T. Zhang, L. Chen and L. Lin, React. Kinet. Catal. Lett. 61 (1997) 391.
[17] F. Solymosi, A. Erdöhelyi and A. Szöke, Catal. Lett. 32 (1995) 43.
[18] D. Wang, J.H. Lunsford and M.P. Rosynek, Topics Catal. 3 (1996) 289.
[19] D. Wang, J.H. Lunsford and M.P. Rosynek, J. Catal. 169 (1997) 347.
[20] F. Solymosi, J. Cserényi, A. Szöke, T. Bánsági and A. Oszkó, J. Catal. 165 (1997) 150.
[21] S.B. Derouane-Abd Ahmed, J.R. Anderson, I. Schmidt, C. Bouchy, C.J.H. Jacobsen and E.G. Derouane, Catal. Today 63 (2000) 461.
[22] C. Bouchy, I. Schmidt, J.R. Anderson, C.J.H. Jacobsen, E.G. Derouane and S.B. Derouane-Abd Ahmed, J. Molec. Catal. A: Chemical 163 (2000) 283.
[23] F. Solymosi, A. Szöke and J. Cserényi, Catal. Lett. 39 (1996) 157.
[24] W. Ding, S. Li, G.D. Meitzner and E. Iglesia, J. Phys. Chem. B 105 (2001) 506.
[25] T. Zhou, A. Liu, Y. Mo and H. Zhang, J. Phys. Chem. A 104 (2000) 4505.
[26] E. Zahidi, H. Oudghiri-Hassani and P.H. McBreen, Nature 409 (2001) 1023.
[27] S.T. Oyama, Catal. Today 15 (1992) 1979.
[28] J. Wang, M. Castonguay, P.H. McBreen, S. Ramanathan and S.T. Oyama, in: *Monograph of the Chemistry of Transition Metal Nitrides and Carbides* (Chapman & Hall, London, 1996) p. 426.
[29] J. Wang, M. Castonguay, J. Deng and P.H. McBreen, Surf. Sci. 374 (1997) 197.
[30] S.T. Wong, Y. Xu, L. Wang, S. Liu, G. Li, M. Xie and X. Guo, Catal. Lett. 38 (1996) 39.
[31] C.D. Wagner, W.M. Riggs, L.E. Davis, J.F. Moulder and G.E. Muilenberg, *Handbook of X-Ray Photoelectron Spectroscopy* (Perkin-Elmer Corporation, Physical Electronics Division, Eden Prairie, MS, 1979).
[32] H. Darmstadt, A. Chaala, C. Roy and S. Kaliaguine, Fuel 75 (1996) 125.